

Supporting Information

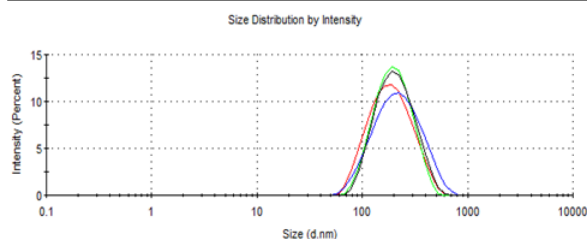
Synthesis of Multifunctional Magnetic NanoFlakes for Magnetic Resonance Imaging, Hyperthermia, and Targeting.

Antonio Cervadoro, Minjung Cho, Jaehong Key, Christy Cooper, Cinzia Stigliano, Santosh Aryal, Audrius Brazdeikis, James F. Leary, and Paolo Decuzzi.*

* Corresponding Author, e-mail: pdecuzzi@houstonmethodist.org

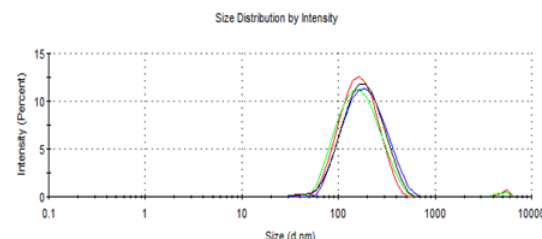
Day 1

	Size (d.nm):	% Intensity:	St Dev (d.nm):
Z-Average (d.nm): 166.0	Peak 1: 202.5	100.0	94.05
PdI: 0.171	Peak 2: 0.000	0.0	0.000
Intercept: 0.922	Peak 3: 0.000	0.0	0.000
Result quality : Good			



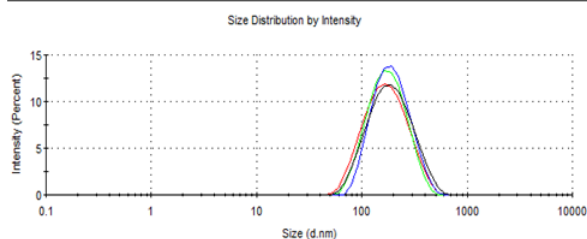
Day 5

	Size (d.nm):	% Intensity:	St Dev (d.nm):
Z-Average (d.nm): 154.3	Peak 1: 176.3	98.6	75.45
PdI: 0.209	Peak 2: 5249	1.0	443.1
Intercept: 0.931	Peak 3: 34.98	0.4	4.221
Result quality : Good			



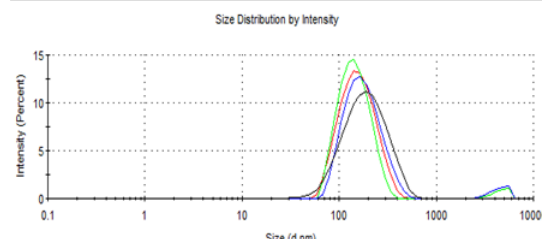
Day 2

	Size (d.nm):	% Intensity:	St Dev (d.nm):
Z-Average (d.nm): 152.6	Peak 1: 185.4	100.0	85.37
PdI: 0.162	Peak 2: 0.000	0.0	0.000
Intercept: 0.932	Peak 3: 0.000	0.0	0.000
Result quality : Good			



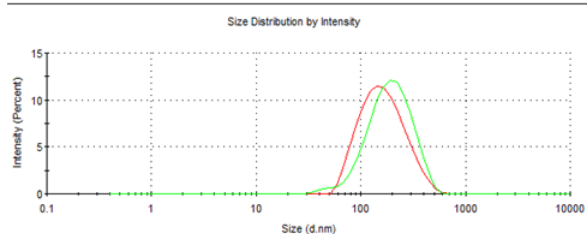
Day 6

	Size (d.nm):	% Intensity:	St Dev (d.nm):
Z-Average (d.nm): 146.6	Peak 1: 165.4	100.0	68.12
PdI: 0.185	Peak 2: 0.000	0.0	0.000
Intercept: 0.927	Peak 3: 0.000	0.0	0.000
Result quality : Good			



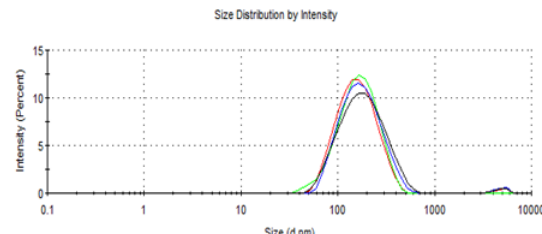
Day 3

	Size (d.nm):	% Intensity:	St Dev (d.nm):
Z-Average (d.nm): 144.5	Peak 1: 177.0	100.0	87.81
PdI: 0.174	Peak 2: 0.000	0.0	0.000
Intercept: 0.924	Peak 3: 0.000	0.0	0.000
Result quality : Good			



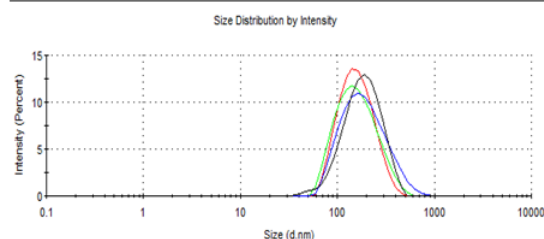
Day 7

	Size (d.nm):	% Intensity:	St Dev (d.nm):
Z-Average (d.nm): 144.4	Peak 1: 170.6	98.7	76.98
PdI: 0.201	Peak 2: 4876	1.3	684.5
Intercept: 0.928	Peak 3: 0.000	0.0	0.000
Result quality : Good			

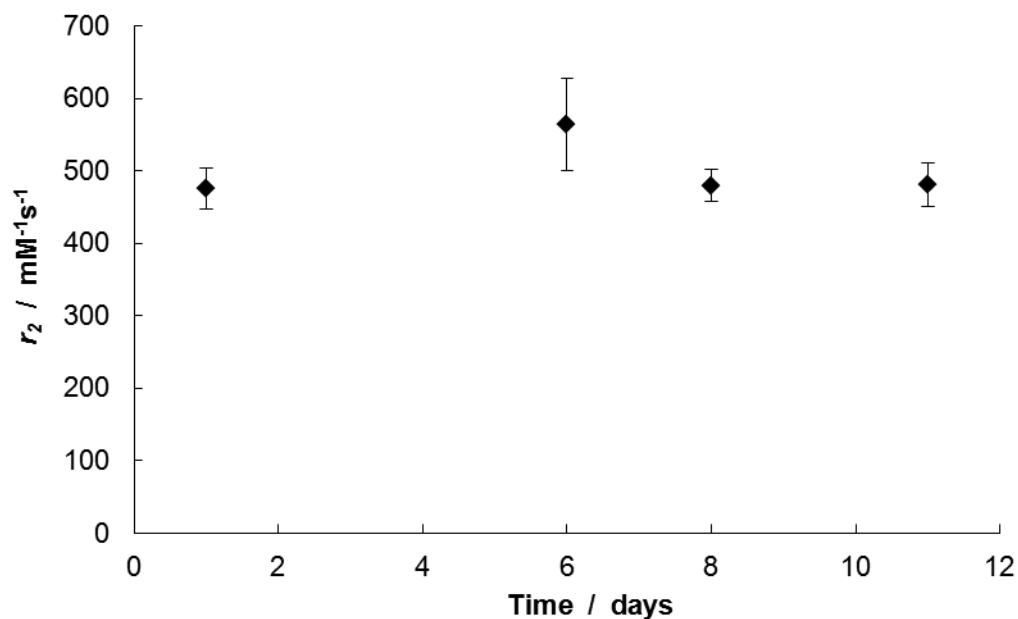


Day 4

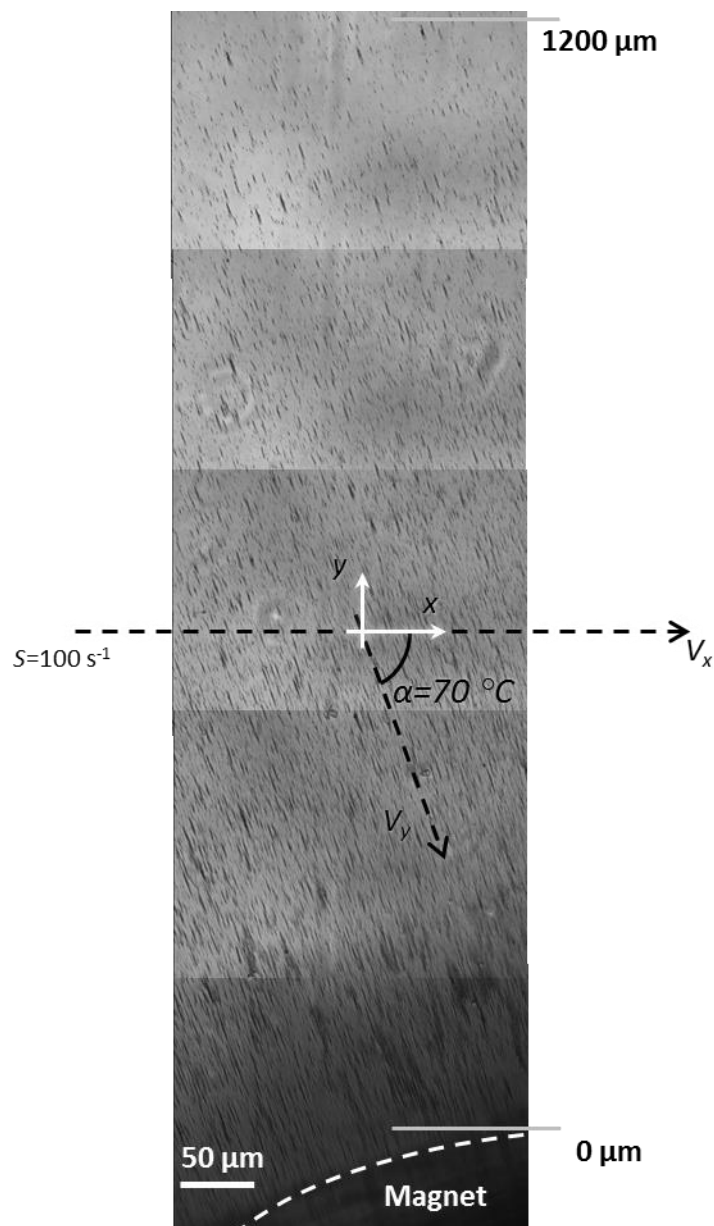
	Size (d.nm):	% Intensity:	St Dev (d.nm):
Z-Average (d.nm): 162.9	Peak 1: 195.2	100.0	82.41
PdI: 0.161	Peak 2: 0.000	0.0	0.000
Intercept: 0.933	Peak 3: 0.000	0.0	0.000
Result quality : Good			



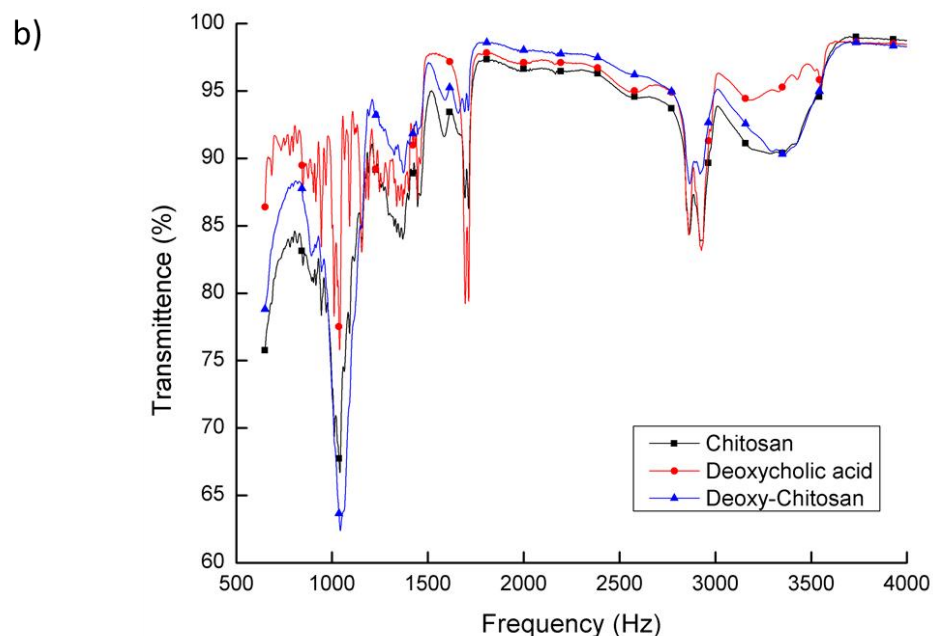
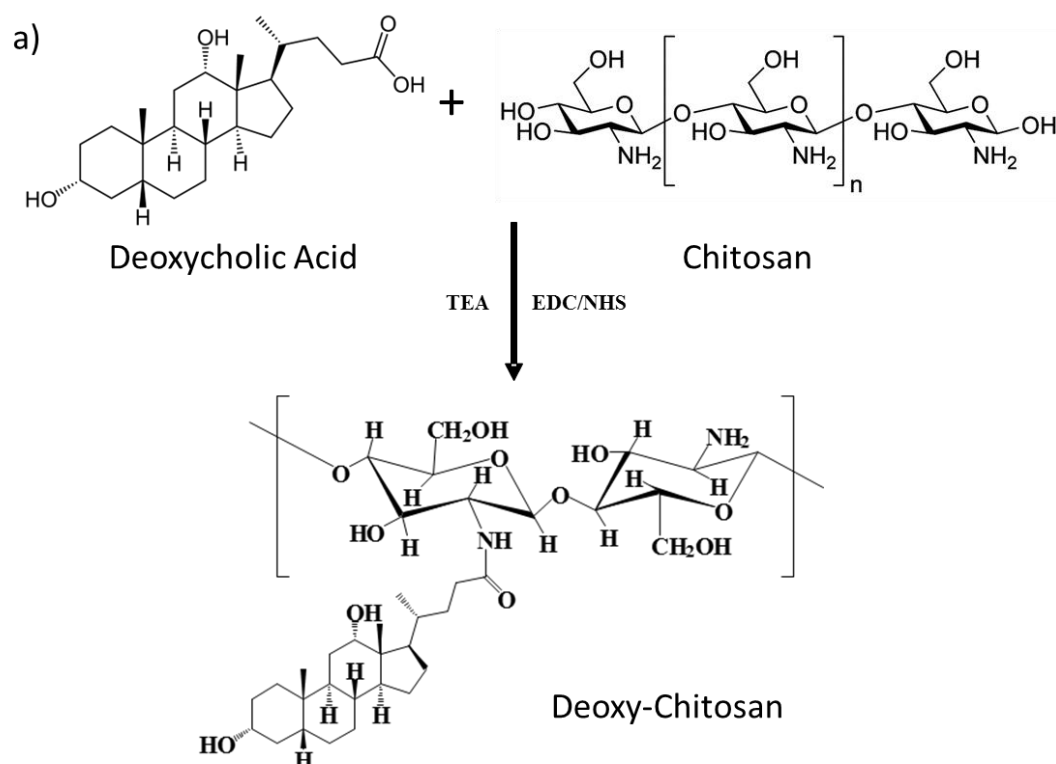
Supp. Figure S1: Dynamic light scattering (DLS) data on the hydrodynamic diameter and polydispersity index (*PDI*) of the MNFs in PBS, at different time points.



Supp. Figure S2: Variation of the transverse relaxivity r_2 over time. The stability of MNFs over time is also demonstrated by the lack of significant variation in transverse relaxivity over 11 days post nanoparticle synthesis.

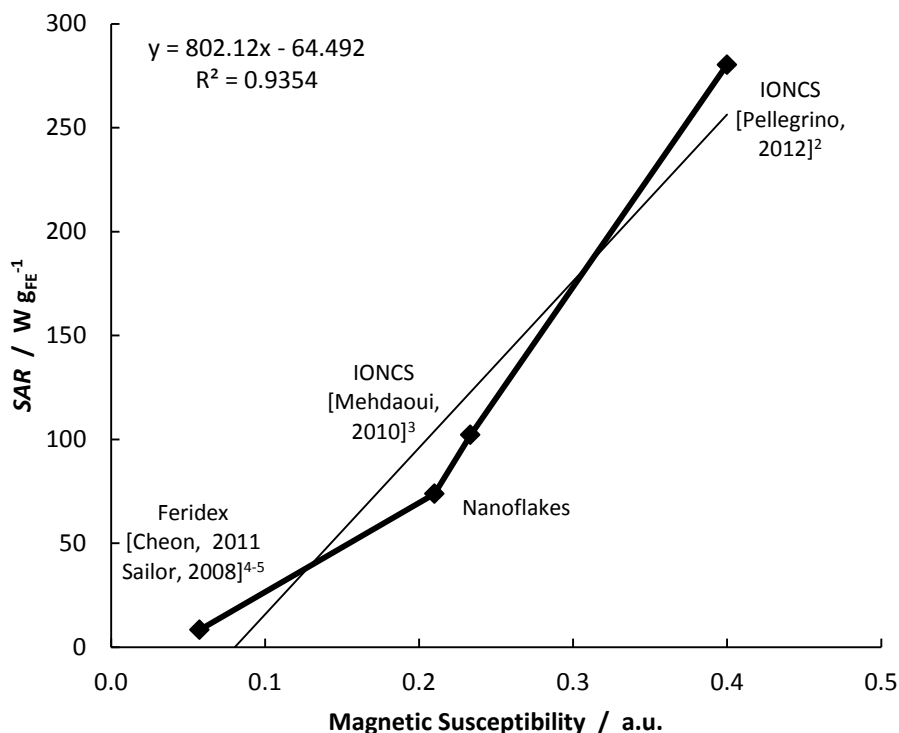


Supp. Figure S3: Cooperative accumulation of MNFs at the bottom of the flow chamber. Note as the MNFs tend to align radially around the magnet (bottom) along the force lines of the field. The growing needle-like architectures of the agglomerating particles demonstrates the cooperative interaction between the MNFs.



Supp. Figure S4: a) Schematic of Deoxy-Chitosan reaction and **b)** FT-IR spectra of chitosan, deoxycholic acid, and chitosan-deoxycholic acid conjugate. The characteristic bands, amide I (1656 cm^{-1}), amide II (1593 cm^{-1}), and amide III (1373 cm^{-1}) of chitosan are intact in both chitosan and chitosan-deoxycholic acid conjugate. However, the H-bonded, N-H stretching, and O-H stretching centered at 3500 cm^{-1} to 3100 cm^{-1} was slightly modified to small intense band at 3446 cm^{-1} along with the broad band, which reduces the extent of the H-bonding due

to the conjugation with deoxycholic acid confirms the formation of the conjugates. Likewise, the absorption of alkyl C-H stretching band of conjugate decreases as compare to that of chitosan at $2950\text{-}2850\text{ cm}^{-1}$ is possibly due to the incorporation of alicyclic rings. In addition, the -O-H stretching band of -COOH group of dexoycholic acid at 2570 cm^{-1} disappeared when conjugated to chitosan further confirms the formation of chitosan-deoxycholic acid conjugates.



Supp. Figure.S5: SAR vs magnetic susceptibility relationship. The specific absorption rate for a broad class of iron oxide nanoparticles (see Figure.5 in the main text) is plotted versus the corresponding value of the magnetic susceptibility. A linear relationship is observed with a high regression coefficient of ($R^2 = 0.8988$ for all nanoparticles; $R^2 = 0.9354$ for all nanoparticles but the particles provided by Sigma-Aldrich). The dependance between SAR and magnetic susceptibility is well defined by the theory:¹

$$SAR = \frac{P}{\rho} = \frac{\pi\mu_0}{\rho} H^2 f \frac{2\pi f \tau}{1 + (2\pi f)^2} \cdot \chi_0(M_s, H)$$

Where we have:

P	Power loss	χ_0	Magnetic susceptibility
H	Magnetic field strength	τ	Particle relaxation time
f	Magnetic field frequency	ρ	Particle density
μ_0	Vacuum magnetic susceptibility	M_s	Saturation magnetization

All the values have been extrapolated by the magnetization data reported by respective authors.²⁻⁵

References

1. Rosensweig, R. E., Heating magnetic fluid with alternating magnetic field. *J. Magn. Magn. Mater.* **2002**, 252 (1-3), 370-374.
2. Guardia, P.; Di Corato, R.; Lartigue, L.; Wilhelm, C.; Espinosa, A.; Garcia-Hernandez, M.; Gazeau, F.; Manna, L.; Pellegrino, T., Water-soluble iron oxide nanocubes with high values of specific absorption rate for cancer cell hyperthermia treatment. *ACS Nano* **2012**, 6 (4), 3080-91.
3. Mehdaoui, B.; Meffre, A.; Lacroix, L. M.; Carrey, J.; Lachaize, S.; Gougeon, M.; Respaud, M.; Chaudret, B., Large specific absorption rates in the magnetic hyperthermia properties of metallic iron nanocubes. *J. Magn. Magn. Mater.* **2010**, 322 (19), L49-L52.
4. Park, J. H.; von Maltzahn, G.; Zhang, L.; Schwartz, M. P.; Ruoslahti, E.; Bhatia, S. N.; Sailor, M. J., Magnetic iron oxide nanoworms for tumor targeting and imaging. *Advanced Materials* **2008**, 20 (9), 1630-1635.
5. Lee, J. H.; Jang, J. T.; Choi, J. S.; Moon, S. H.; Noh, S. H.; Kim, J. W.; Kim, J. G.; Kim, I. S.; Park, K. I.; Cheon, J., Exchange-coupled magnetic nanoparticles for efficient heat induction. *Nat. Nanotechnol.* **2011**, 6 (7), 418-22.